LANGMUIR

Interfaces: Adsorption, Reactions, Films, Forces, Measurement Techniques, Charge Transfer, Electrochemistry, Electrocatalysis, Energy Production and Storage

Direct Measurement of the Magnitude of van der Waals interaction of Single and Multilayer Graphene

Yu-Cheng Chiou, Tuza Olukan, Mariam Ali Almahri, Harry Apostoleris, Cheng-Hsiang Chiu, Chia-Yun Lai, Jin-You Lu, Sergio Santos, Ibraheem Almansouri, and Matteo Chiesa

Langmuir, **Just Accepted Manuscript** • DOI: 10.1021/acs.langmuir.8b02802 • Publication Date (Web): 23 Sep 2018

ACS Publications

is published by the American Chemical Society. 1155 Sixteenth Street N.W., Washington, DC 20036

Direct Measurement of the Magnitude of van der Waals interaction of Single and Multilayer Graphene

Yu-Cheng Chiou[1*], Tuza Adeyemi Olukan[2*], Mariam Ali Almahri[2], Harry Apostoleris[2], Cheng Hsiang Chiu[2],Chia-Yun Lai[2], Jin-You Lu[2],Sergio Santos[3], Ibraheem Almansouri[2], Matteo Chiesa[2,4]

[1]Topco Scientific Co. Ltd., No.483, Sec. 2, Tiding Blvd., Neihu, Taipei City 11493, Taiwan

[2]Laboratory for Energy and NanoScience (LENS), Khalifa University of Science and Technology, Masdar Institute Campus, Abu Dhabi, UAE

[3]Future Synthesis AS Uniongata 18, 3732 Skien, Norway

[4]Arctic Renewable Energy Center (ARC),Department of Physics and Technology, UiT The Artic University of Norway, Norway

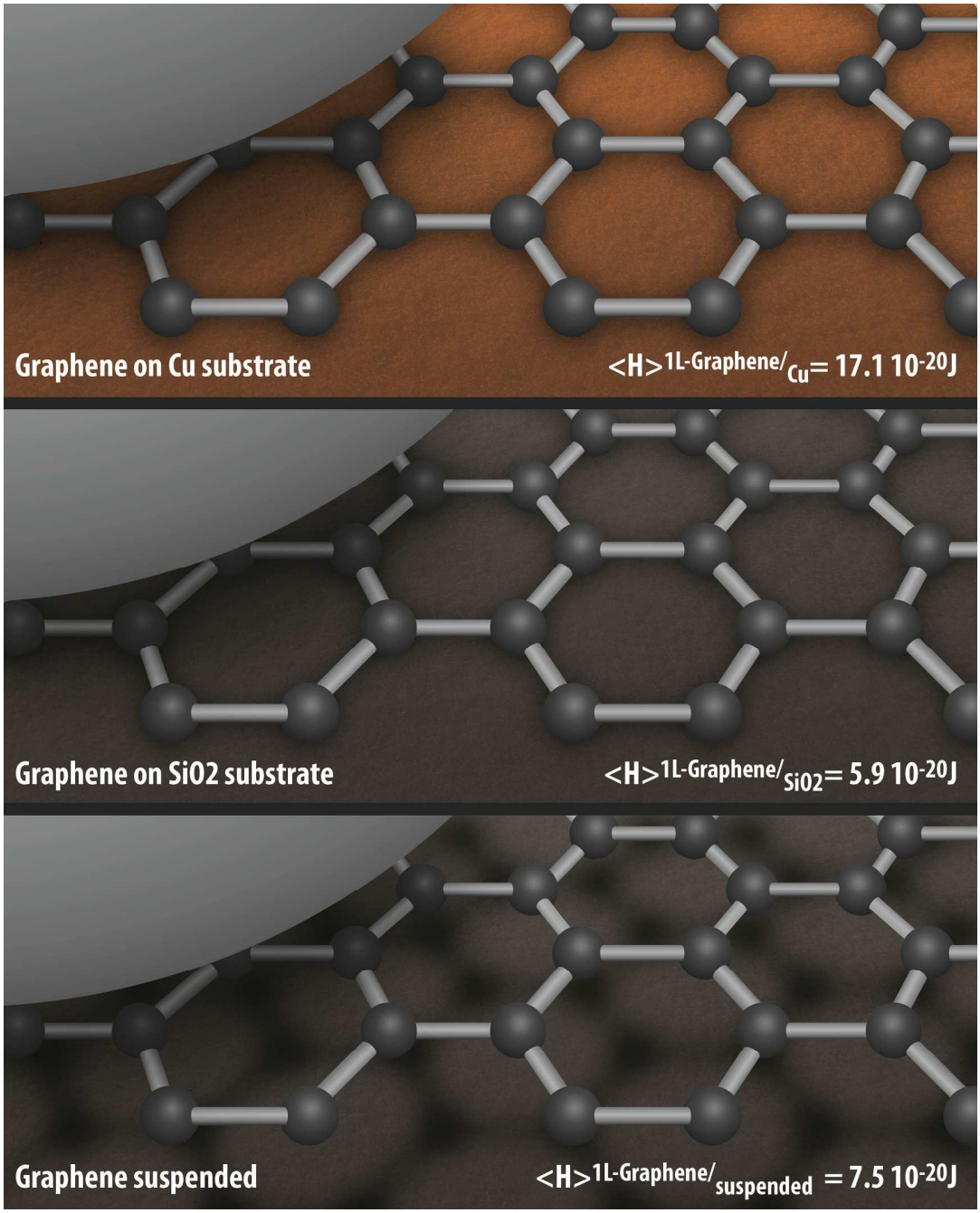
Graphene on Cu substrate
<H>1L-Graphene/Cu= 17.1 10-20J
Graphene on SiO2 substrate
<H>1L-Graphene/SiO2= 5.9 10-20J
Graphene suspended
<H>1L-Graphene/suspended = 7.5 10-20J

TOC

Abstract

Vertical stacking of monolayers via van der Waals assembly is an emerging field that opens promising routes toward engineering physical properties of two-dimensional (2D) materials. Industrial exploitation of these engineering heterostructures as robust functional materials still requires bounding their measured properties so to enhance theoretical tractability and assist in experimental designs. Specifically, the short-range attractive van der Waals forces are responsible for the adhesion of chemically inert components and are recognized to play a dominant role in the functionality of these structures. Here we reliably quantify the strength of ambient van der Waals forces in terms of an effective Hamaker coefficient for CVD-grown graphene and show how it scales by a factor of two or three from single to multiple layers on standard supporting surfaces such as copper or silicon oxide. Furthermore, direct measurements on freestanding graphene provide the means to discern the interplay between the van der Waals potential of graphene and its supporting substrate. Our results demonstrated that the underlying substrates could be controllably exploited to enhance or reduce the van der Waals force of graphene surfaces. We interpret the physical phenomena in terms of a Lifshitz theory-based analytical model.

Introduction

The development of graphene and the entire class of 2D materials[1-2] over the last decade has raised tantalizing application possibilities that leverage on the unique physics of 2D crystal structures to engineer materials at the nanoscale. In recent years interest in this area has turned towards the concept of "van der Waals heterostructures[3]," in which multiple 2D layers are stacked with precise orientations to yield the desired properties. An example relates to electronic band gaps which can be tuned by varying the constituent layers and their orientation[4-6]. 2D layers can be seen as building blocks to construct novel atomic scale metamaterials[7] that open up a new paradigm of "2D manufacturing". In short, new structures are engineered from the atomic level up by the combination of 2D building blocks to yield the desired properties. Besides their atomic flatness, such structures are unique in that the component layers join by other than chemical bonds. The so called "glue" that binds these blocks is the ubiquitous van der Waals VdW force[8] that arises from plane to plane interactions. The VdW forces are therefore bringing 2D manufacturing of materials to fruition in a very elegant and unorthodox way. In this work we quantify the VdW interaction of CVD-grown graphene by means of the Hamaker coefficient that quantifies the strength of the VdW interactions. Hamaker[9] demonstrated that the VdW force between two bodies could be split into a purely geometrical component and a parameter that depends solely on material chemistry i.e. polarizabilities and atomic densities of the atoms in the two interacting bodies[9]. The material chemistry is contained in the Hamaker coefficient, that is here treated as a coefficient because of the small interaction range that we consider. We use the standard terminology and term this coefficient A. Lifshitz[10] presented a more rigorous approach that incorporated the many-body effects neglected by Hamaker and based on thermodynamic

considerations of the interacting bodies as a continuum described by dielectric properties. As the VdW interaction ultimately results from the fluctuations of the electromagnetic field between two macroscopic bodies, the Lifshitz theory can still be described by an effective Hamaker coefficient A[11]. In this way, A offers a more general picture of surface properties than other measured physical quantities such as adhesion or surface energy. Despite the clear relevance of these forces to understand the interactions of 2D structures, the Hamaker coefficient - and indeed the VdW force profiles that it generates - of graphene and other 2D materials remains poorly studied. In particular, we refer to direct quantification that allows to gain experimental access to physical insight while keeping the experiments relatively simple. There is a lack of studies even if the volume of work dedicated to this investigation is substantial[12-14]. For example, while there have been many papers in the literature that have provided numerical experimental values for the Hamaker coefficient of similar systems based on AFM experiments, these rely very strongly on approximations and low throughput, so robust validation is many times lacking[15]. Other methods are otherwise overcomplicated and might provide indirect methods to quantify VdW forces rather than a single parameter that provides physical insight such as the Hamaker coefficient[16]. In the present work we directly quantify the van der Waals interactions of graphene surfaces by using the observables of a recently developed[15, 17] bimodal AFM methodology to map the Hamaker coefficient in the non-retarded regime[11].We note that an important factor in surface characterization of 2D materials, which we account for in this study, is the impact of the substrate on the measured values. As the sample thickness is in the order of Angstroms, surface force measurements may be influenced by the underlying substrate as well as by the sample. We perform measurements of samples on a variety of substrates to evaluate the impact of the substrate on the measured VdW strength of the 2D graphene systems. We note that the

experimental methodology followed to produce the samples might be of relevance for future experimentation and results critical in isolating to real measured forces. We have employed nanofabrication techniques to create patterned substrates that support regions of free-standing graphene where the graphene-substrate distance is in the order of microns. By performing measurements on these suspended regions, we characterize the graphene itself, thus removing the effect of the substrate. With these results we have succeeded in directly measuring the VdW strength of graphene surfaces on the nanoscale. We emphasize however that the values that we provide in this work are relevant to ambient conditions implying that they are not ideal. That is, deviation from ideal Hamaker coefficient values might result from the presence of pollutants, inter-layer water presence or other.

Experiment

The graphene for our measurements is grown on Cu substrates in-house via chemical vapor deposition (CVD). Varying the gas precursor flow rates as described in the methods section controlled the number of layers. Confirmation of the number of graphene layers was done by Raman spectroscopy via the ratio of the 2D and G peaks in a Raman spectrum, which varies from about 3 in single-layer graphene and decreases to less than 1 in multilayer samples[18-19]. We take Raman spectra of both graphene-on-Cu (as-grown) and graphene transferred onto both flat SiO_2 and patterned SiO_2 substrates that support regions of suspended graphene as described in the introduction. The patterned substrate was created via focused ion beam etching to create a pattern of "holes" over which the graphene layers are transferred (details in supplementary). In

this way, atomic force microscopy (AFM) measures the Hamaker of graphene alone emerging from these suspended regions and without the influence of the substrate.

After the Raman measurements, deposited and transferred graphene samples were measured by AFM where 100x100nm^2 maps of the surface were collected in bimodal operation (see Methods section). The mapped regions fell inside the area where the Raman spectrum was taken. The Hamaker coefficient was mapped based on a method described in detail in previous works[17, 20] and summarized in the methods section here. In summary, the Hamaker coefficient A can be derived from raw bimodal AFM observables obtained directly from images. That implies that each pixel from the AFM image results in a value of A thus preserving both resolution and speed. The expression is:

$$A = -\frac{3\pi k_2 A_{02}\cos(\varphi_2)}{0.83RQ_2A_2}\sqrt{d_{min}^5 A_1} \qquad (1)$$

where R is the tip radius, k_m and Q_m the spring constant and quality factor of the mth mode respectively, d_{min} the minimum distance of approach, A_m the oscillation amplitude of the mth mode and A_{0m} the free amplitude of the mth mode. Only the first and the second modes, i.e. m=1 and m=2, are to be excited as typical in bimodal AFM. We further note that the minimum distance of approach d_{min} refers to the minimum tip-surface distance per cycle. That is, as the cantilever oscillates there is one minimum distance in each complete cycle. Such minimum distance is what we term d_{min}. The expression we employ correspond to the approximation $d_{min} \approx z_c - A_1$ where z_c is the mean cantilever-surface distance. It is also worth noting that there will always be a true minimum tip-surface distance coinciding with an intermolecular distance a_0. These distances are typically taken to be 0.16-0. 2 nm (we take 0.165 nm in our derivations) and imply that matter cannot interpenetrate due to electron cloud repulsion. Thus, when we write $d_{min}=0$ the implication is that there has already been mechanical contact and tip-surface

deformation equal to a_0. In addition to the bimodal mapping, force spectra were taken in standard single-mode operation. The force vs. distance profiles were reconstructed using the Sader-Jarvis-Katan method from which an effective Hamaker coefficient can be obtained by fitting the attractive part of the force with an inverse squared power law. In addition to these experimental measurements we performed density functional theory (DFT) simulations to generate, from first principles, force-distance profiles for 1-, 2- and 3-layer suspended graphene. The simulations assisted in our interpretation by providing cause-effect controllable relationships even though we acknowledge the limitations of such prediction in experimental set-ups. In fact, such limitations motivate our experimental study that turns to direct experimental quantification.

Results

The value of the Hamaker coefficient for graphene on Cu is mapped as shown in Figure 1. The three Hamaker coefficient maps, Figure 1a, b, c, show regions of single, double and multi-layer graphene as confirmed by Raman spectra, Figure 1e. Hamaker coefficient values for each pixel are extracted and the distribution of these values for each of the three samples is reported in Figure 1d. The results show for the first time a clear difference between the VdW strength of mono, bi and multi-layer graphene. Moreover, the Hamaker coefficient maps provide an indication of graphene continuity at far higher resolution (nm scale) than Raman spectroscopy. This provides additional insight into the origin of the observed Hamaker coefficient values. For example, the regions in the maps of single and multi-layer graphene where the measured

Hamaker coefficient abruptly changes, are likely to represent Cu grain boundaries that would impact graphene growth and the measured strength of the VdW interaction. Clearly the mean Hamaker coefficient values are affected by the substrate, as the variations in the measured values between the grain boundaries and bulk crystal regions demonstrates. Thus, the Hamaker coefficient values are to be looked upon as effective values that include the effect of the substrate. Considering further the influence of the substrate, we note that the substrate itself can be modified during the CVD process (e.g. by promoting hydrogenation of the surface). While it is clear that the influence of the substrate on measured graphene surface properties presents an additional challenge for characterization, it also provides an extra degree of freedom to selectively modifying the effective properties of graphene. That is, one must specify the substrate in order to understand the properties of graphene. The implication is that graphene, in that sense, should not be considered as the whole of the physical entity from which properties arise. Thus, it must be reported as a substrate-graphene system instead. Furthermore, growth processes may also play a role, the differences in the measured surface properties between different graphene samples may, in this understanding, be in part related to differences in the substrate induced by the variations in the growth process. The trends observed in Figure 1 are confirmed with different samples and different tips of radius $R < 7$ nm[20] (see methods section) .

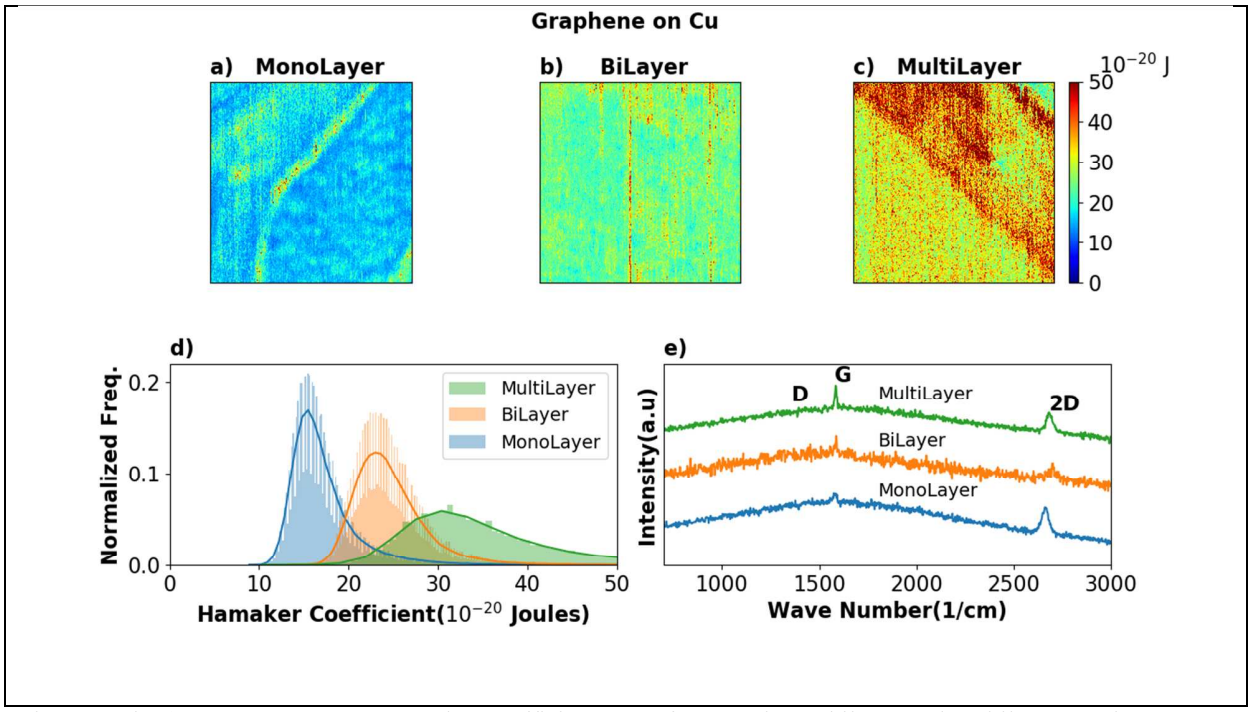

Figure 1a, b, c) 100 nm × 100 nm Hamaker coefficient maps for monolayer, bilayer and multilayer graphene on Cu substrate respectively. d) Distribution of Hamaker coefficient values belonging to monolayer, bilayer and multilayer graphene. The Hamaker coefficient distributions present the raw data where no filter is applied see SI. e) Raman spectra plots of regions where monolayer, bilayer and multilayer graphene are identified. No filter is applied and the curves represent the raw data collected. The 532nm laser source has a spot size with radius ≈ 5 μm making the area extension several order of magnitude larger than the Hamaker coefficient maps see SI.

Figure 2 shows a summary of the Hamaker coefficient distributions and Raman spectra for mono, bi and multilayer samples on all of the substrates considered, namely Cu in Figure 2a, b, SiO_2in Figure 2c, d and freestanding graphene Figure 2e, f (see supporting information). One of the first observations one can derive from the results in Figure 2 is the reduced strength of the VdW forces for non-metal substrate or freestanding graphene. Strikingly, the measured Hamaker coefficient for graphene on SiO_2 is lower than that for the suspended graphene with no substrate at all. We hypothesize that this reduced Hamaker coefficient might relate to variations in the

dielectric/refractive properties of the effective Silicon-graphene surface alone, rather than in material density since it is clear that the presence of the substrate would lead to an additive atom density increase according to Hamaker's method. Roughly speaking wave interference might lead to absorption and emission resonance affecting the effective dielectric constant of the Hamaker-substrate surface. We will provide experimental evidence supporting this claim below. One can also notice in Figure 2d, a strong peak just below 1000cm^{-1}, which indicates the presence of the SiO_2substrate. The strong Raman signal in the region 800-1000cm^{-1} may also indicate the presence of PMMA residual. This last assumption cannot be entirely ruled out. On the other hand, the dominating contribution is from the SiO_2 substrate itself. As explained in the SI file, the transfer process is tedious and may also leave residuals of water between the graphene and the SiO_2 in addition to PMMA. The presence of a strong SiO_2 signal though might suggest that the presence of a strong SiO_2 signal between 900 and 1000 cm^{-1} serving as a proof that our graphene is successfully transferred and coated on SiO_2 substrate. It is possibly to have some water residuals at the graphene/SiO_2 interface, and the presence of residual could further provide some screening effect and thus reduce the measured effective Hamaker coefficient, however this reduction in the effective Hamaker coefficient on non-metal substrates can be explained even without invoking screening effect of the PMMA residue or water, as will be elaborated later in the manuscript

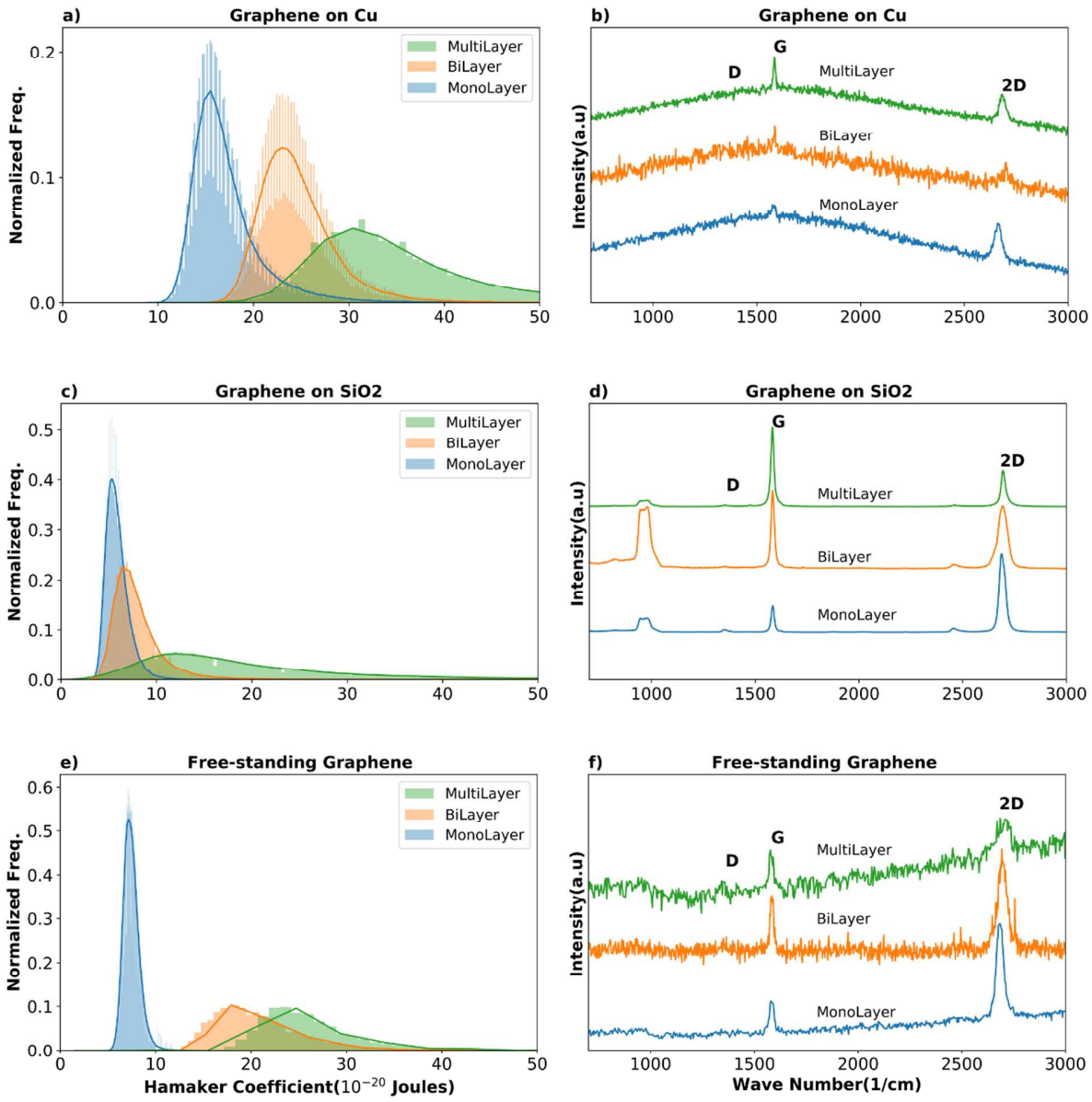

Figure 2a, c, e) Distribution of Hamaker coefficient values belonging to the different Hamaker coefficient maps directly measured by bimodal AFM and comparison to Raman spectra for graphene on Cu, SiO_2 and free standing b, d, f). It is worth noticing that the Raman spectra represent an area that is almost 3 orders of magnitude greater that the area observed in our AFM maps.

For SiO_2 substrate, Figure 2c, and the freestanding graphene Figure 2e, the distribution for the monolayer sample is very sharp indicating a high homogeneity of the graphene film, while in the

case of bilayer and multilayer samples the distributions are much broader indicating possible heterogeneity in the graphene coverage. As before, this heterogeneity can be observed thanks to the high spatial resolution of our Hamaker coefficient maps where regions of single, double and multi-layer graphene can be observed see Figure 3a, b, c and SI for more details. The suspended graphene has no noticeable SiO_2 signal reinforcing the fact that the graphene is sufficiently isolated from the substrate and can be considered as free standing[21]. Figure 2e also exhibits a clear distinction between monolayer and bilayer graphene directly quantifying the interlayer van der Waals interaction strength. The distinction between bilayer and multilayer graphene is less pronounced for the suspended graphene, but similar trends are observed in all the samples. Furthermore, it is worth reflecting on how the substrate influences the Hamaker coefficient maps versus the results in the Raman spectrum. In the Raman, the Cu substrate presence is detected as noise that reduces the overall signal-to-noise ratio and cannot be effectively decoupled. However, in the Hamaker coefficient, the substrate increases, in the case of metal substrates, and decreases, in the case of non-metal substrate, the total measured value of the effective Hamaker coefficient, providing a means to quantify the strength of the probe-substrate interaction. Therefore, this approach offers the possibility of separating the measured surface properties into a graphene-dependent and a substrate-dependent component.

Before proceeding our results are corroborated by collecting force-distance profiles for the suspended graphene (see Figure 3d). The Hamaker coefficient values derived by fitting the force-profile in Figure 3d with an inverse squared power law (in line with the assumption of a force distance relationship $F \approx RA/d^2$) were 11×10^{-20} J, 17×10^{-20} J and 36×10^{-20} J for the monolayer, bilayer and multiple layer respectively. We recall that 100s of data points were

collected for each force curve and the values we provide are the mean values obtained in the experiments. These values fall inside the Hamaker coefficient distributions reported in Figure 2e and obtained in bimodal AFM. The results further corroborate that the Hamaker coefficient values obtained with the two different methods, i.e. force reconstruction and bimodal mapping, are statistically consistent.

We further corroborate our experimental observations by means of DFT calculations. The computationally expensive DFT AFM scanning is performed with a typical pyramid silicon tip on graphene surface by using PBE-D2 method. Owing to the limited DFT simulation domain, we use the pyramid silicon tip with a dangling bond at the apex and hydrogen terminated base rather than a real AFM tip. However, the used pyramid silicon tip is able to generate similar magnitude as the experimental AFM tip did during the DFT AFM scanning, even if its size is much smaller than that of experimental AFM tip[22]. The DFT derived interaction energy and force-distance profiles are reported in the Figure 3d and SI respectively, where interaction energy $\Delta E(d) = E_{tot}(d) - E_{tip} - E_{graphene}$ between the tip and the graphene layers are directly taken from the energy difference between the total system with different tip-surface distance and individual tip/graphene. The force profiles are taken from the gradient of total energy of the tip-graphene system, which is given by $\boldsymbol{F} = -\nabla(E_{tot}(d))$. As the number of graphene layers increases, the magnitude of the adhesion force and Hamaker coefficient also increase. We acknowledge that in the description of graphene-related systems, the PBE-D2 method gives less accuracy as compared to the van der Waals functional methods, such as vdW-DF2-C09[23], due to its simplified pair-wise force field; however, the DFT-AFM predicted force-distance curves still give reasonable agreement with the experimental data, as indicated by Fig. 3(d-e).

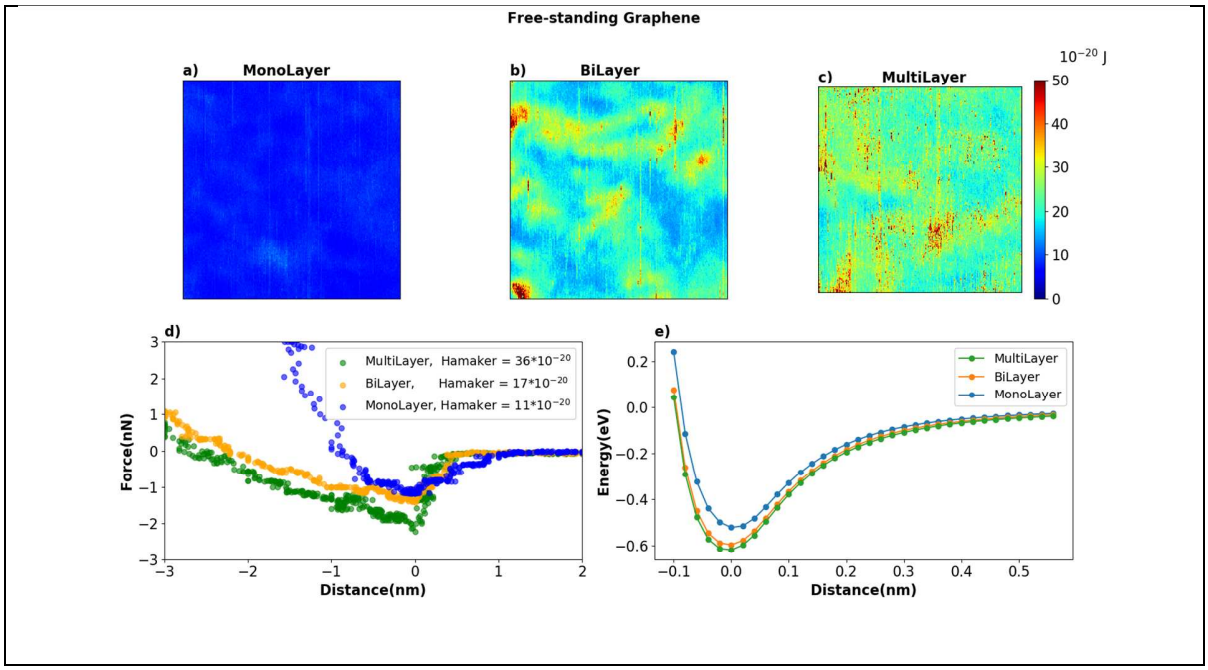

Figure 3a, b, c) 100 nm × 100 nm Hamaker coefficient maps for free-standing monolayer, bilayer and multilayer graphene respectively. d)Force profile for Monolayer, Bilayer and Multilayer suspended graphene samples reconstructed by AM-AFM. e) DFT predicted interaction energy vs distance of tip to freestanding graphene with different layers see SI for more information.

While useful for confirming trends, the DFT simulations are not so well suited to investigate the role of the substrate; consider the computational intensiveness of the problem. In order to discern the effect of the substrate we revert to an analytical effective Hamaker coefficient model based on the Lifshitz theory. The complicated geometrical problem in the derivations is avoided by assuming that the interaction energy between the AFM tip and graphene coated substrate is similar to that between a flat silica substrate and graphene coated substrate. By considering the relative refractive index of silica, graphene[24], and substrate, the equations can be separated into two simplified equations for metal and non-metal substrates, respectively, by taking two leading terms. The detailed derivations are included in Supporting Information.

$$F = -\frac{A_{eff} R}{6L^2} \cong -\frac{A_{402} R}{6L^2} - \frac{A_{102} R}{6(L+b)^2} \quad (2)$$

$$F = -\frac{A_{eff} R}{6L^2} \cong -\frac{A_{402} R}{6L^2} - \frac{A_{102} R}{6(L+b)^2} \left(\frac{n_1^2 - n_4^2}{n_1^2 + n_4^2} / \frac{n_1^2 - n_0^2}{n_1^2 + n_0^2}\right) \quad (3)$$

where A_{eff} is the effective Hamaker coefficient, A_{402} is the Hamaker coefficient between AFM tip and graphene in air (obtained by our experiment see Figure 2 e since data is no available) and A_{102} is the Hamaker coefficient between the SiO_2 tip and Substrate in air. Equation 2 and 3 refer respectively to metal and non-metal substrates (see SI for the derivations). Let R be the tip radius, *L* be the distance between graphene and AFM tip, *b* the graphene thickness and η the retractive index where the meaning of the suffixes 0-4 is given below. The values of *L* and *b* corresponding to monolayer graphene sample are 3.8Å and 3.35 Å, respectively, as predicted by our DFT simulations. In this work, materials 0, 1, 2, and 4 are vacuum/air, substrate (Cu or SiO_2), SiO_2, and graphene, respectively. To calculate the effective Hamaker coefficient, the parameter A_{402} is taken from the experimental values of the suspended graphene since to our knowledge no value is available in the literature (see Table I). The values of A_{102} are taken from the Hamaker coefficient of Cu[25]and SiO_2[25], respectively. The comparison with the experimental (AFM measured) Hamaker coefficients, are shown in Table I. In the table, we provide the mean values obtained over 65 k data points (approx.) and the standard deviation. We also account for systematic errors in the measurements that might result from the calibration of the spring constant, the tip radius, the optical lever sensitivity and other. In our system the lever sensitivity error might be up to 5%, and together with the tip radius calibration, this is probably the highest source of systematic errors in our experiments. All parameters that have length units in our equations are affected by the lever sensitivity error. We have assumed however that the overall

error, including any propagations, is approximately 5%. While this is by far not a conservative approach, it gives an indication of the range in the uncertainty in the mean that we provide, i.e. in all cases the error is several times smaller than the standard deviation. Random errors would be much smaller due to the large number of data points that we have acquired and can be ignored. The error in the mean accounting for this 5% is provided in Table I in parenthesis in all cases. Despite the great deal of assumptions necessary to feed equations (2) and (3), our calculations on copper agree surprisingly well with experimental data. On the SiO_2 substrate, the prediction qualitatively agrees with the experimental data despite being less accurate. This reduced accuracy may be due to the residuals left on the surface or between the surfaces by the transfer process (PMMA and water respectively), that we do not account for in our model. Nevertheless, the model captures the fact that the effective Hamaker coefficient of graphene on SiO_2 substrate is weaker than those of suspended graphene layers, something that can be explained by the negative value of $(\frac{n_1^2-n_4^2}{n_1^2+n_4^2}/\frac{n_1^2-1}{n_1^2+1})$ for SiO_2 substrate (refractive index n_1~1.45), which indicates that the VdW force on top of the graphene layer is reduced by the SiO_2 substrate while it is enhanced on the metal substrates.

Table I. A comparison of effective Hamaker coefficient between experiment and our theoretical prediction. The mean and standard deviation are provided in the table. The number in the parenthesis indicates the upper band of the systematic errors which is mostly due to the error in the measurement of the sensitivity of the cantilever, i.e. approximately 5%[26-27].

Method	Substrate	Monolayer	Bilayer	MultiLayer

		10^{-20} J	10^{-20} J	10^{-20} J
Experiment	Suspended	7.5±0.8 (0.4)	20.9±6.1 (1.0)	26.9±12.8 (1.3)
	Cu	17.1±3.8 (0.9)	24.6±4.1 (1.23)	36±12.3 (1.8)
	SiO_2	5.9±1.2 (0.3)	8.0±3.1 (0.4)	21.3±16.2 (1.1)
Calculation	Cu	15.22	21.71	26.87
	SiO_2	4.16	16.58	23.92

This also explains in terms of van der Waals potentials the wetting transparency of monolayer graphene reported in the literature[28] since the measured effective Hamaker coefficient for the monolayer graphene on the Cu substrate, reported in Table I, is strikingly similar to the tabulated value for Hamaker coefficient of the SiO_2-Cu pair, i.e. 15.6[11].

Furthermore, our findings support a recently proposed hypothesis that tries to provide an analytic thermodynamic criterion for subsequent layer CVD-growth that depends among others on the VdW interaction energies[29].The large number of reports on CVD-growth of graphene on metal substrate shows how this process is routinely achieved and extendable to large-scale fabrication[30-33] thanks to the strong van der Waals potential of the metal substrates support that constructively help in the growth of monolayer graphene. This is not the case for SiO_2substrates. Equation 3 points out that if not properly matched (refractive index), the substrate may reduce the strength of the van der Waals interaction thereby inhibiting direct CVD-growth of single monolayers. Despite the oversimplification of equation 3 and realizing that there are many more effects that might independently participate in the overall phenomena, equation 3 can be used as a general rule of thumb to assess whether direct CVD-growth on non-metal substrate is feasible simply by looking at the substrate refractive index.

Conclusions

Direct measurement of the strength of the VdW forces of graphene has long been challenging, posing a problem for the application of graphene and other 2D materials, whose most promising potential uses (e.g. "VdW stack" applications) often depend on the precise manipulation of surface forces. In this study we have leveraged on the power of atomic force microscopy to measure the Hamaker coefficient of in-house-grown CVD graphene samples, thereby quantifying the strength of the VdW interaction. The use of AFM allows the Hamaker coefficient to be directly probed with nanoscale resolution, addressing a significant difficulty in prior studies which is the inability to distinguish "true" properties of single, double and triple layer graphene from the average properties that a measurement with low spatial resolution will detect when characterizing a sample with micro- or nano-scale variations in the graphene thickness. To resolve a further challenge, the effect of the substrate on the measured surface forces, we have conducted studies on different substrates, including a specially-fabricated substrate that supports regions of suspended graphene where the effect of the substrate is eliminated. DFT calculations are used to corroborate the measurements and show qualitative agreement with our observations on suspended graphene. An analytical model is developed from the theory of Lifshitz to explain the observed values and provide a means of quantifying the impact of the substrate, leading to the recognition that the substrate may, depending on its dielectric properties, either significantly reduce or enhance the VdW interaction measured at the graphene surface. The AFM-based techniques described here, as they can be easily implemented in any laboratory, without sophisticated equipment or involved sample preparation, provide a means of efficiently collecting large quantities of data that will be valuable in resolving the persistent questions and

uncertainties regarding the surface properties of graphene and other 2D materials. We emphasize however that the values that we provide in this work are relevant to ambient conditions implying that they are not ideal. That is, deviation from ideal Hamaker coefficient values might result from the presence of pollutants, inter-layer water presence or other.

Methods

Graphene growth:

We use a planar TECH planarGROW-2S thermal CVD system with parallel heaters to synthesize graphene on Cu foil substrates. Sigma Aldrich Cu substrates (25 μm thick, 2× 2 cm2, 99.999% pure) for all experiments. Cu foils were cleaned prior to each growth by sonication for a total of 10 min in acetone, IPA, and DI water sequentially followed by drying (nitrogen blowing) before loaded into the CVD chamber. The growth of mono-layer graphene was carried out with a relatively low methane flow rate of 2 sccm and a hydrogen flow rate of 20 sccm at 1000 °C. The process starts by annealing the copper substrate surface for 15 min using hydrogen flow (5 sccm, 0.1 Torr, and 1000 °C). Following the high-temperature annealing, methane is introduced to the process for 120 minutes (2 sccm, 0.2 Torr, and 1000 °C), with a hydrogen flow of 20 sccm. Before cooling the chamber, an additional growth process was introduced to obtain graphene layers stacking in one sample. A higher methane flow (20 sccm, 2 Torr, and 1000 °C) was then introduced for 5 minutes while the hydrogen flow remained the same at 20 sccm. After the two-step growth process, the exposure to methane and hydrogen, the sample was cooled to room temperature and removed. See SI for more information.

Table II: Graphene deposition parameters

Step	Time (minutes)	Hydrogen	Methane	Temperature	Pressure
1st step	120	20	2	1000 °C	0.2
2nd step	5	20	20	1000 °C	2

Graphene transfer:

We use a standard process whereby the graphene-on-Cu sample is spin coated with PMMA and then immersed in an aqueous solution of ferric chloride to etch the Cu. When the Cu is dissolved in the etchant, the graphene/PMMA stack is transferred into DI water to remove the unwanted Cu residues. Finally, the exposed graphene side is brought into contact with the SiO_2 substrate and the PMMA is etched away in acetone.

Raman Analysis:

A Witec Alpha 300 RAS Raman spectroscopy with 532nm laser source is employed in our experiments. During the measurement, the laser spot size diameter is kept constant and measures approximately 5 μm.

AFM cantilever calibration:

The cantilevers are calibrated through thermal analysis in the proximity of the sample surface (~50 nm). The resonance frequencies were obtained by fitting the thermal peaks. The software provided by Asylum Research would then automatically calculating the spring constant and the quality factor.

Bimodal operation:

An Asylum Research Cypher AFM and standard AC240TS cantilevers with spring constants k, Q factors and resonant frequencies f of $k_{(1)}\approx$ 1.5-3 N/m, $k_{(2)}\approx$ 60-90 N/m, $Q_{(1)}\approx$ 100, $Q_{(2)}\approx$ 400, $f_{(1)}\approx$ 70 kHz and $f_{(2)}\approx$ 450 kHz were employed. The subscripts stand for mode number, i.e. 1 and 2. Standard AC240TS cantilevers were oscillated at the first 2 modal resonance frequencies while the frequencies were determined with thermal analysis when the cantilevers were close to the sample surface (~30nm). Cypher AFM was set to operate in attractive regime, that is, first mode free amplitude A_{01} was set at ~$0.5A_c$ and the setpoint was set at ~$0.7A_{01}$[15, 17]. First two modes' oscillation amplitude and phase channel (A_1, A_2, φ_1, and φ_2) were recorded. We then employed

$$d_{\min}-\left[\left[\frac{3\pi k_{(2)}A_{02}Q_{(1)}\cos\phi_{(2)}}{0.83k_{(1)}A_{01}Q_{(2)}\cos\phi_{(2)}}\right]^{2/3}\frac{A_1}{(A_2)^{2/3}}\right]d_{\min}^{2/3}+2A_1=0 \qquad (4)$$

and Eq. 1 to obtain Hamaker coefficient values. See SI for more information.

Since the Hamaker coefficient is a parameter that we derive from the force at a distance, one would wonder what the distance really is for a rough substrate. Topography variations could in principle cancel out by Hamaker coefficient variations over such effective area. We recently recovered apparent height losses using such principles[34]. On the other hand, we assume in our model an effective flatness for the tip-sample area of interaction acknowledging that apparent variations in A could indeed occur in such area due to topographically induced artifacts. A general introduction of bimodal AFM can refer to the work by Garcia *et al*[35].

Force reconstruction:

A Cypher AFM from Asylum Research was operated in amplitude modulation (AM) mode and standard AC240TS cantilevers (k ≈ 2N/m, Q ≈ 100, and f0 ≈ 70 kHz) were used for all the AFM experiments. For force reconstruction, sample rate of 1 Hz, free oscillation amplitude ≈70 nm, and trigger point of 68nm were used. This relatively high set point enables us to avoid the bistability between the attractive and repulsive region during tip approach and yields a smooth transition between the two regimes. Amplitude A and phase φ versus tip-sample separation distance d were recorded to employ the Sader-Jarvis-Katan formalism[36-38] to reconstruct the conservative forces. Since it is well-known that the tip radius R significantly affects the tip-sample interaction force, R was monitored in all experiments with critical amplitude (A_c) method[20] to make sure that R remains constant throughout the experiment. A minimum of 100 force profiles is reconstructed on each sample on at least 5 different locations within each sample.

Experimental errors and validation of results

Force curve profiles consist of mapping the net force, one to one, to the tip surface distance. Force curve profiles[39] are typically exploited in AFM to quantify parameters such as adhesion, surface energy and Hamaker coefficient, even though the latter is typically indirectly obtained from the adhesion force or other[14]. While indirect measurements of VdW forces have been studied from such force profiles for almost 50 years[40], these are still relatively slow and imply taking a force curve point by point and recovering the desired parameter by either inspection of the curve, fitting a model with approximations where there are more unknowns than expressions, or a combination of both. The advent of dynamic AFM for force reconstruction allowed

obtaining experimental points from the full range of distances, including distances close to the nm where instability had been a major issue that typically led to data loss[38, 41-42].

In summary, force curves, especially in quasi-static AFM, have several disadvantages in terms of errors and throughput. First, the cantilever might snap into contact and the relevant information that would be otherwise obtained near the surface, i.e. below a few nm of distance, is lost. This has clear implications for recovering the Hamaker coefficient at such distances which are, in fact, the main distances discussed in our work. Second, since force curves, both in the quasi-static and in the dynamic modes, take times in the order of 1 second to be obtained, statistics and approximations are typically exploited. It is, in any case, time consuming and statistically significant results might involve many hours of data collection. In our recently developed bimodal method, the Hamaker coefficient is mapped pixel by pixel as an image is collected, or straight after collection. For example, a 256 by 256 pixel image of 1μm^2 will take approximately 5 minutes to be collected. The processing of the data will take approximately 1 extra minute if not done simultaneously – we note we processed the data after collection. That implies that approximately 60 k data points can be collected from the inspected area in minutes. The distributions resulting from the 60 k points are approximately Gaussian (see Fig. 1). Standard statistics can be easily performed on these distributions, i.e. such as providing the mean, median and standard deviations to summarize and interpret the data. A summary of the results is given in the table below.

Table III. Summary of the distributions of data obtained in bimodal AFM for the figures shown in the article. We summarize the distributions which are close to Gaussian with the mean, standard deviation (std) and median values below.

	MonoLayer (10^{-20} J)	BiLayer (10^{-20} J)	MultiLayer (10^{-20} J)
Graphene on Cu	mean = 17.1 median = 16.3 std = 3.8	mean = 24.6 median = 24.0 std = 4.1	mean = 36.0 median = 33.2 std = 12.3
Graphene on SiO2	mean = 5.9 median = 5.7 std = 1.2	mean = 8.0 median = 7.4 std = 3.1	mean = 21.3 median = 16.5 std = 16.3
Free-standing Graphene	mean = 7.5 median = 7.4 std = 0.8	mean = 20.9 median = 19.9 std = 6.1	mean = 26.9 median = 25.1 std = 12.8

On the other hand, repeatability and reproducibility might still be an issue. With reproducibility and repeatability, we mean to consider the conditions for which the data, including the mean and standard deviation values, will be compatible with future experiments carried out under similar conditions. The force reconstruction also consisted of 100 data points per sample and per experiment. We have previously demonstrated[43] that this results in robust mean and standard deviation values for this type of experiment including reproducibility and repeatability.

To deal with this repeatability and reproducibility for the bimodal experiments we conducted the force reconstruction experiments and the bimodal experiments over ten times with different tips and samples. The patterns and results presented in our Fig. 1 and 2 were consistent. In this sense our experiments were consistent throughout all data acquisition.

Reference

1. Novoselov, K. S.; Jiang, D.; Schedin, F.; Booth, T. J.; Khotkevich, V. V.; Morozov, S. V.; Geim, A. K., Two-dimensional atomic crystals. *Proc. Natl. Acad. Sci. U.S.A.* **2005,** *102* (30), 10451-10453.
2. Novoselov, K. S.; Geim, A. K.; Morozov, S. V.; Jiang, D.; Zhang, Y.; Dubonos, S. V.; Grigorieva, I. V.; Firsov, A. A., Electric Field Effect in Atomically Thin Carbon Films. *Science* **2004,** *306* (5696), 666-669.
3. Geim, A. K.; Grigorieva, I. V., Van der Waals heterostructures. *Nature* **2013,** *499*, 419.
4. Yankowitz, M.; Xue, J.; Cormode, D.; Sanchez-Yamagishi, J. D.; Watanabe, K.; Taniguchi, T.; Jarillo-Herrero, P.; Jacquod, P.; LeRoy, B. J., Emergence of superlattice Dirac points in graphene on hexagonal boron nitride. *NatPh* **2012,** *8*, 382.
5. Liu, L.; Feng, Y. P.; Shen, Z. X., Structural and electronic properties of h-BN. *Physical Review B* **2003,** *68* (10), 104102.
6. Giovannetti, G.; Khomyakov, P. A.; Brocks, G.; Kelly, P. J.; van den Brink, J., Substrate-induced band gap in graphene on hexagonal boron nitride: Ab initio density functional calculations. *Physical Review B* **2007,** *76* (7), 073103.
7. Novoselov, K. S.; Mishchenko, A.; Carvalho, A.; Castro Neto, A. H., 2D materials and van der Waals heterostructures. *Science* **2016,** *353* (6298).
8. Margenau, H., Van der waals forces. *Reviews of Modern Physics* **1939,** *11* (1), 1-35.
9. Hamaker, H. C., The London—van der Waals attraction between spherical particles. *Physica* **1937,** *4* (10), 1058-1072.
10. Lifshitz, E., The theory of molecular attractive forces between solids. *Sov.Phys.JETP* **1956,** *2*, 73-83.
11. Bergström, L., Hamaker constants of inorganic materials. *Advances in Colloid and Interface Science* **1997,** *70*, 125-169.
12. Hammer, M. U.; Anderson, T. H.; Chaimovich, A.; Scott Shell, M.; Israelachvili, J., The search for the hydrophobic force law. *Faraday Discuss.* **2010,** *146*, 299-401.
13. Krajina, B. A.; Kocherlakota, L. S.; Overney, R. M., Direct determination of the local Hamaker constant of inorganic surfaces based on scanning force microscopy. *The Journal of chemical physics* **2014,** *141* (16), 164707.
14. Israelachvili, J., *Intermolecular & Surface Forces*. 2 ed.; Academic Press: New York, 1991.
15. Lai, C.-Y.; Santos, S.; Chiesa, M., Systematic Multidimensional Quantification of Nanoscale Systems From Bimodal Atomic Force Microscopy Data. *ACS nano* **2016**.
16. Kasai, H.; Tolborg, K.; Sist, M.; Zhang, J.; Hathwar, V. R.; Filsø, M. Ø.; Cenedese, S.; Sugimoto, K.; Overgaard, J.; Nishibori, E.; Iversen, B. B., X-ray electron density investigation of chemical bonding in van der Waals materials. *Nature materials* **2018,** *17* (3), 249-252.

17. Lai, C.-Y.; Perri, S.; Santos, S.; Garcia, R.; Chiesa, M., Rapid quantitative chemical mapping of surfaces with sub-2nm resolution. *Nanoscale* **2016**.
18. Ferrari, A. C.; Meyer, J. C.; Scardaci, V.; Casiraghi, C.; Lazzeri, M.; Mauri, F.; Piscanec, S.; Jiang, D.; Novoselov, K. S.; Roth, S.; Geim, A. K., Raman Spectrum of Graphene and Graphene Layers. *Phys. Rev. Lett.* **2006,** *97* (18), 187401.
19. Ni, Z.; Wang, Y.; Yu, T.; Shen, Z., Raman spectroscopy and imaging of graphene. *Nano research* **2008,** *1* (4), 273-291.
20. Santos, S.; Guang, L.; Souier, T.; Gadelrab, K.; Chiesa, M.; Thomson, N. H., A method to provide rapid in situ determination of tip radius in dynamic atomic force microscopy. *Review of Scientific Instruments* **2012,** *83* (4), 043707.
21. Geim, A. K., Graphene: Status and Prospects. *Science* **2009,** *324* (5934), 1530-1534.
22. Pérez, R.; Payne, M. C.; Štich, I.; Terakura, K., Role of Covalent Tip-Surface Interactions in Noncontact Atomic Force Microscopy on Reactive Surfaces. *Phys. Rev. Lett.* **1997,** *78* (4), 678-681.
23. Hamada, I.; Otani, M., Comparative van der Waals density-functional study of graphene on metal surfaces. *Physical Review B* **2010,** *82* (15), 153412.
24. Jussila, H.; Yang, H.; Granqvist, N.; Sun, Z., Surface plasmon resonance for characterization of large-area atomic-layer graphene film. *Optica* **2016,** *3* (2), 151-158.
25. Visser, J., On Hamaker constants: A comparison between Hamaker constants and Lifshitz-van der Waals constants. *Advances in colloid and interface science* **1972,** *3* (4), 331-363.
26. Song, Y.; Wu, S.; Xu, L.; Fu, X., Accurate Calibration and Uncertainty Estimation of the Normal Spring Constant of Various AFM Cantilevers. *Sensors* **2015,** *15* (3).
27. Slattery, A. D.; Blanch, A. J.; Quinton, J. S.; Gibson, C. T., Accurate measurement of Atomic Force Microscope cantilever deflection excluding tip-surface contact with application to force calibration. *Ultramicroscopy* **2013,** *131*, 46-55.
28. Rafiee, J.; Mi, X.; Gullapalli, H.; Thomas, A. V.; Yavari, F.; Shi, Y.; Ajayan, P. M.; Koratkar, N. A., Wetting transparency of graphene. *Nature materials* **2012,** *11* (3), 217-22.
29. Ye, H.; Zhou, J.; Er, D.; Price, C. C.; Yu, Z.; Liu, Y.; Lowengrub, J.; Lou, J.; Liu, Z.; Shenoy, V. B., Toward a Mechanistic Understanding of Vertical Growth of van der Waals Stacked 2D Materials: A Multiscale Model and Experiments. *ACS nano* **2017,** *11* (12), 12780-12788.
30. Addou, R.; Dahal, A.; Sutter, P.; Batzill, M., Monolayer graphene growth on Ni(111) by low temperature chemical vapor deposition. *Appl. Phys. Lett.* **2012,** *100* (2), 021601.
31. Ago, H.; Ito, Y.; Mizuta, N.; Yoshida, K.; Hu, B.; Orofeo, C. M.; Tsuji, M.; Ikeda, K.-i.; Mizuno, S., Epitaxial Chemical Vapor Deposition Growth of Single-Layer Graphene over Cobalt Film Crystallized on Sapphire. *ACS nano* **2010,** *4* (12), 7407-7414.
32. Sutter, E.; Albrecht, P.; Sutter, P., Graphene growth on polycrystalline Ru thin films. *Appl. Phys. Lett.* **2009,** *95* (13), 133109.
33. Johann, C.; Alpha, T. N. D.; Martin, E.; Carsten, B.; Dirk, W.; Niemma, B.; Frank, J. M. z. H.; Raoul van, G.; Bene, P.; Thomas, M., Growth of graphene on Ir(111). *NJPh* **2009,** *11* (3), 039801.
34. Chia-Yun, L.; Sergio, S.; Matteo, C., Reconstruction of height of sub-nanometer steps with bimodal atomic force microscopy. *Nanotechnology* **2016,** *27* (7), 075701.
35. Garcia, R.; Proksch, R., Nanomechanical mapping of soft matter by bimodal force microscopy. *European Polymer Journal* **2013,** *49* (8), 1897-1906.
36. Sader, J. E.; Jarvis, S. P., Accurate formulas for interaction force and energy in frequency modulation force spectroscopy. *Appl. Phys. Lett.* **2004,** *84* (10), 1801-1803.
37. John, E. S.; Takayuki, U.; Michael, J. H.; Alan, F.; Yoshikazu, N.; Suzanne, P. J., Quantitative force measurements using frequency modulation atomic force microscopy—theoretical foundations. *Nanotechnology* **2005,** *16* (3), S94.

38. Katan, A. J.; van Es, M. H.; Oosterkamp, T. H., Quantitative force versus distance measurements in amplitude modulation AFM: a novel force inversion technique. *Nanotechnology* **2009,** *20* (16), 165703.
39. Butt, H. J.; Cappella, B.; Kappl, M., Force measurements with the atomic force microscope: Technique, interpretation and applications. *Surface Science Reports* **2005,** *59* (1–6), 1-152.
40. The direct measurement of normal and retarded van der Waals forces. *Proceedings of the Royal Society of London. A. Mathematical and Physical Sciences* **1969,** *312* (1511), 435-450.
41. Giessibl, F. J., Forces and frequency shifts in atomic-resolution dynamic-force microscopy. *Physical Review B* **1997,** *56* (24), 16010-16015.
42. Lai, C.-Y.; Olukan, T.; Santos, S.; Al Ghaferi, A.; Chiesa, M., The power laws of nanoscale forces under ambient conditions. *Chem. Commun.* **2015,** *51* (99), 17619-17622.
43. Chang, Y.-H.; Olukan, T.; Lai, C.-Y.; Santos, S.; Lin, T.-Y.; Apostoleris, H.; Font, J.; Barcons, V.; Chiesa, M., Establishing Nanoscale Heterogeneity with Nanoscale Force Measurements. *The Journal of Physical Chemistry C* **2015,** *119* (32), 18267-18277.

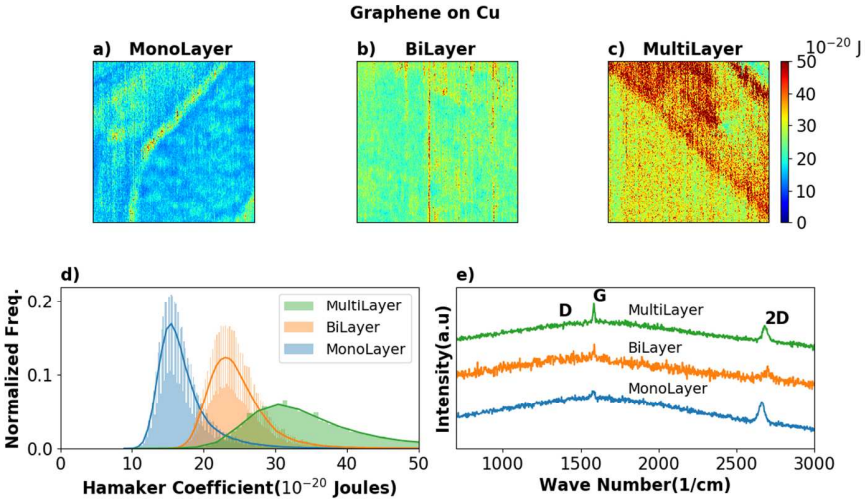

Figure 1

330x171mm (100 x 100 DPI)

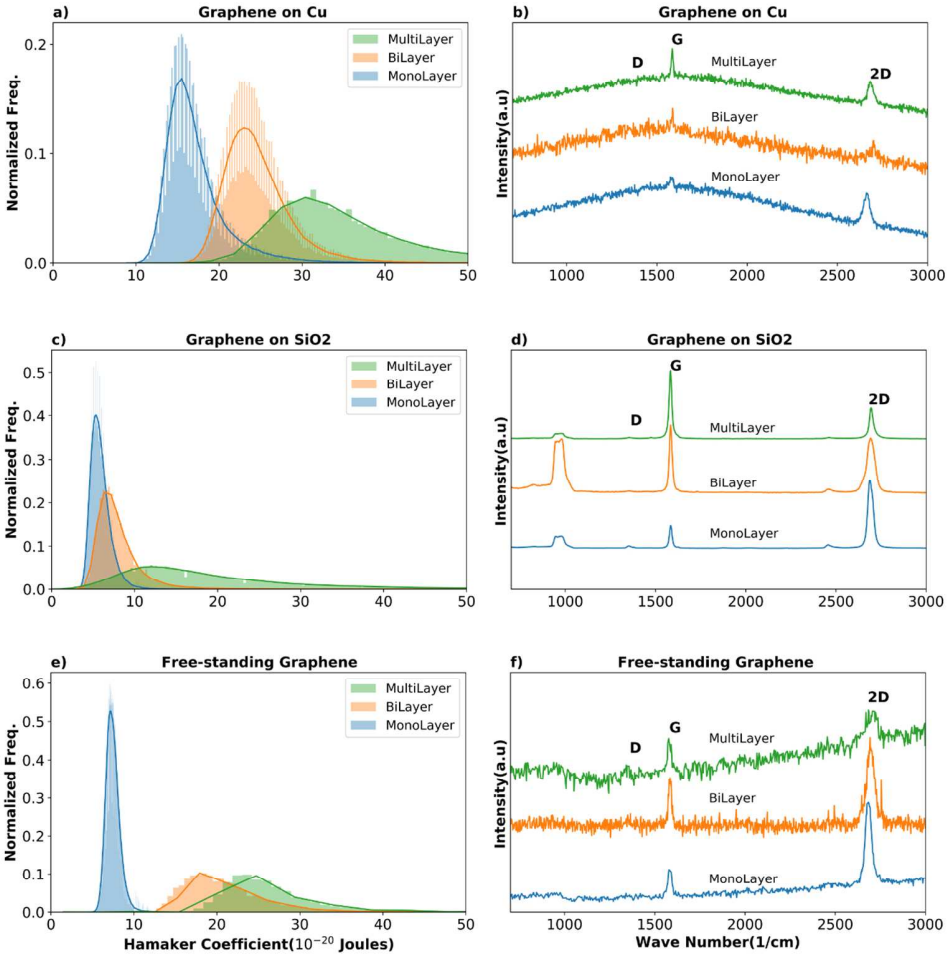

Figure 2

360x368mm (96 x 96 DPI)

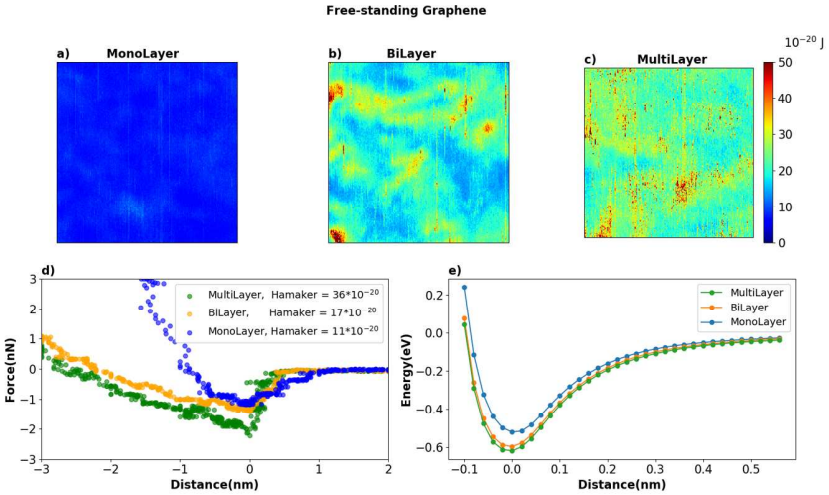

Figure 3

490x260mm (96 x 96 DPI)

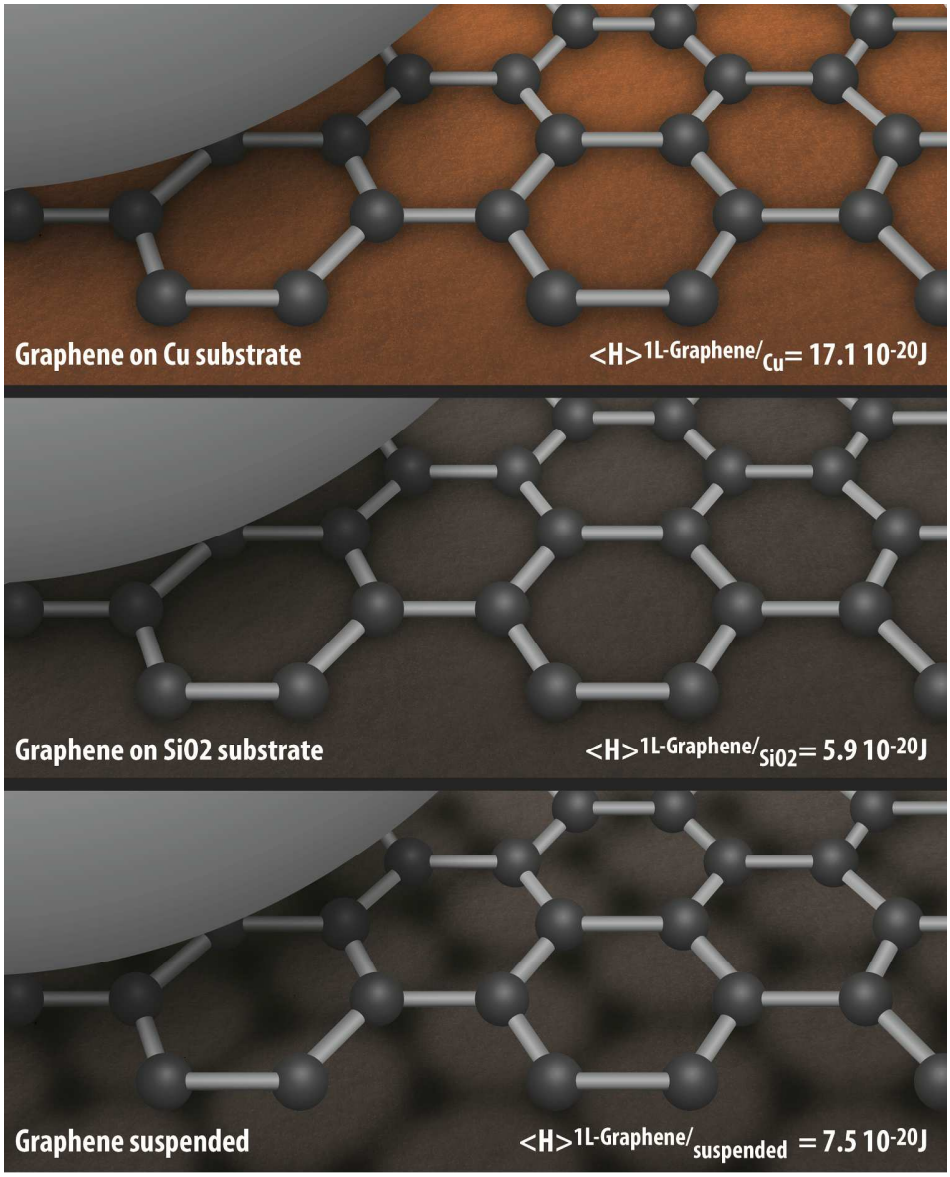

TOC

209x259mm (300 x 300 DPI)